**Program Digest, 2019 IEEE International Ultrasonics Symposium (IUS)**
**Glasgow, Scotland, October 6-9, 2019**

# A comparison of natural and acoustic radiation force induced shear wave propagation speed measurements in open-chest pigs

Lana B.H. Keijzer[1,*], Jason Voorneveld[1], Dan J. Bowen[1], Mihai Strachinaru[1], Antonius F.W. van der Steen[1,2], Nico de Jong[1,2], Johan G. Bosch[1], Hendrik J. Vos [1,2], Annette Caenen[1,**]
[1]*Department of Cardiology, Erasmus MC, Rotterdam, the Netherlands*
[2]*Department of Imaging Physics, Delft University of Technology, Delft, the Netherlands*
[*]l.b.h.keijzer@erasmusmc.nl, [**]a.caenen@erasmusmc.nl

***Abstract* — Different shear wave elastography methods have been proposed to measure cardiac material properties. This study compared shear waves naturally generated by aortic and mitral valve closure to those externally induced with an acoustic radiation force throughout the cardiac cycle. The shear wave timing and propagation speeds were measured in four pigs with open-chest recordings. Despite spatial and temporal differences in excitation source, the propagation speeds of the natural shear waves were found to be in the same range as the propagation speeds of the active shear waves. The results also suggested a large inter-beat variability for the natural shear waves.**

***Keywords—cardiac shear wave elastography, aortic valve closure, mitral valve closure, acoustic radiation force***

## I. Introduction

Shear wave elastography (SWE) comprises all techniques that measure tissue stiffness based on shear wave propagation characteristics. In the last decade, several SWE methods have been proposed to evaluate the material properties of the heart for assessment of cardiac function. Two clinical SWE methods have been recently reported [1]–[3]: (i) active SWE, analyzing externally induced shear waves (SWs) after applying an acoustic radiation force (ARF) and (ii) passive SWE, studying natural SWs in the heart such as SWs excited by aortic and mitral valve closure (AVC, MVC). These studies demonstrated the clinical feasibility of both types of SWE for cardiac stiffness characterization. Nevertheless, clear differences exist between active and passive SWs. For passive SWE, time and location of activation are dictated by the valve closures, while this is flexible for active SWE. Furthermore, the SW's temporal and spatial characteristics are expected to be different in both methods due to differences in the source of mechanical excitation.

To get insights into the correlation between active and passive SWs in the heart, we studied both SW types in the same subjects by evaluating shear wave propagation speed (SWS) as a function of time. This is done in an open-chest pig setting in order for active SWE to be able to capture the stiffness variations over the full cardiac cycle [4].

This work is part of the STW – Dutch Heart Foundation partnership program 'Earlier recognition of cardiovascular diseases' with project number 14740, which is (partly) financed by the Netherlands Organization for Scientific Research (NWO).

## II. Methods

### A. Experimental Set-up

SWE measurements were performed on four pigs (Yorkshire x Norwegian landrace), as approved by the Erasmus MC Animal Experiments committee (17-2411-03, 18-5224-01). Two pigs that were included in the study had diabetes mellitus, hypercholesterolemia and chronic kidney disease. After anesthesia, full sternotomy was performed, and the animals were mechanically ventilated while lying on their back. SWE measurements were acquired with an ATL P4-2 probe connected to the fully programmable ultrasound research system Vantage 256 (Verasonics, Kirkland, WA) after receiving a trigger based on the pig's ECG R-peak.

### B. Data Acquisition

An acquisition consisted of two consecutive elastography sequences, each individually ECG triggered. Both sequences aimed at the interventricular septum (IVS) in a long-axis parasternal view. The first sequence used high frame rate (HFR) diverging waves (DW) to measure the passive SWs after AVC and MVC during 2 s. The second sequence actively induced SWs in the IVS using an ARF impulse repeatedly (42 times over a duration of 1.2 s). One ARF-based measurement completed in 20 – 28 ms and consisted of three steps: (i) HFR DW for reference, (ii) a focused pushing beam to excite SWs and (iii) HFR DW again to image the propagation of the SWs. Radio frequency (RF) data of both sequences were saved for offline processing.

To optimize data quality, different settings have been tested for the DW imaging and ARF pushes based on previous reported SWE settings in [5], [6]. For the DW measurements, a pulse-inversion transmission sequence or a 3-angle DW compounding scheme was implemented. The virtual focus of the DW sequence was either -34 mm or -288 mm. The pulse repetition rate varied between 6.7 kHz and 10.4 kHz, resulting in frame rates between 2.2 kHz and 9.3 kHz. The ARF pushes had a length of 400 µs and a center frequency of 2 MHz or 2.8 MHz. The focal depth of the ARF was adjusted to the location of the IVS.

### C. Data Analysis

The RF data were beamformed to obtain analytic data and subsequently, a one-lag autocorrelation technique was applied

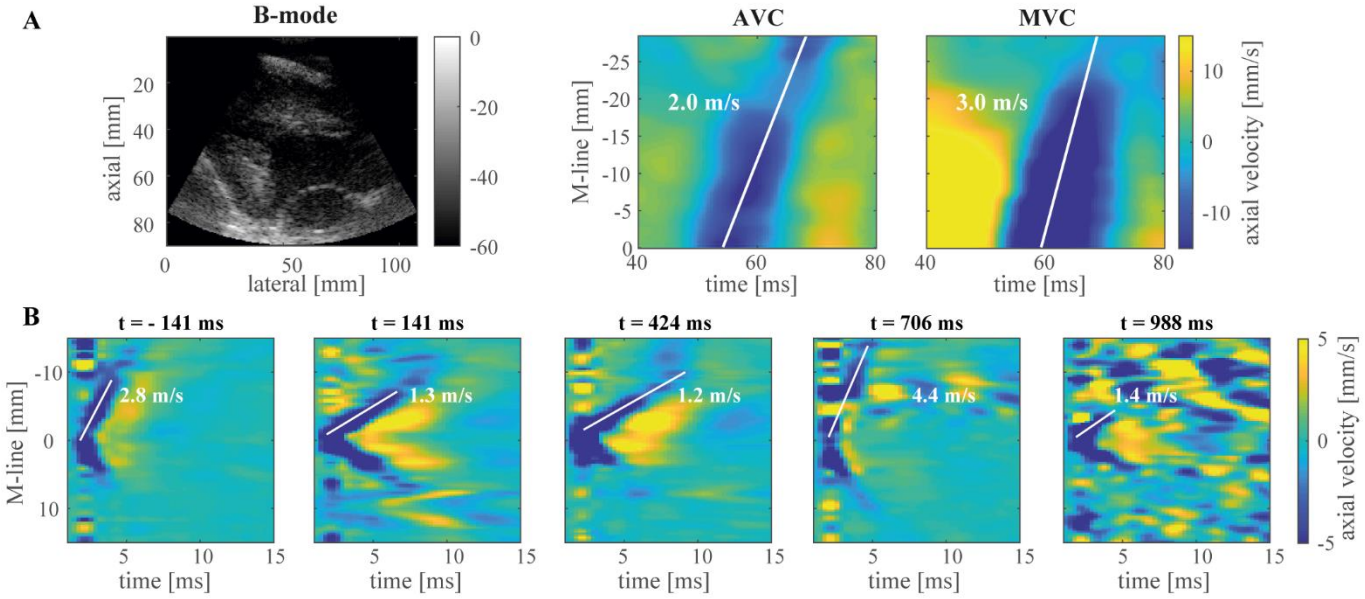


Fig. 1. A) Example of two M-panels for the SWs induced after AVC and MVC in Pig 1 and the corresponding B-mode image. B) Example of the varying propagation speeds found over the cardiac cyle with an active SW sequence in Pig 1. The moments of occurrence of the individual M-panels (titles) are with respect to the manually-selected onset of diastole (t=0).

to obtain axial particle velocities [7]. Anatomic M-mode lines (M-lines) were manually drawn as splines across the IVS to create M-panels, displaying the axial particle velocities along these M-lines as a function of acquisition time. For every SW measurement, 10 M-lines were manually drawn (5 M-lines each by two observers). As the frequency content and SNR of active and passive SWs differed, we applied different post-processing settings for each sequence, as described below.

*1) Passive SWE*

To minimize the effect of blood motion and noise, a 6th order Butterworth low-pass filter (cutoff frequency of 250 Hz) was applied on the IQ data. After calculating the one-lag autocorrelation frames before computing the phase [7], the data were smoothed using a Gaussian spatial smoothing filter of 5.6˚ by 3.0 mm. A 6th order Butterworth 15 – 100 Hz bandpass filter was subsequently applied on the estimated tissue velocities in the Cartesian domain. The moments of AVC and MVC were determined from the B-mode images and the corresponding Tissue Doppler images (TDI). SWS was subsequently estimated using a normalized Radon transform on the M-panels, resampled to an equal number of pixels in space and time [8].

*2) Active SWE*

Before tissue velocity estimation, a Gaussian spatial smoothing filter of 1.8˚ by 1.0 mm in the polar domain was applied to reduce the effect of noise. The reverberation frames (~400 µs) directly after the individual ARF pushes were removed. Then, linear interpolation was used to replace the missing frames between the reference and remaining frames after the induced SWs. Next, a 6th order 75 – 750 Hz Butterworth bandpass filter was applied to the M-panels to reduce gross motion and high frequency noise. The SWS values were then determined manually by drawing a straight line from the ARF push focus towards the apex along the negative peak TDI velocities in the M-panel. The slope of this line corresponded to the SWS.

The invasive nature of the measurements posed several challenges regarding the steadiness of the probe on a moving heart and the orientation of the probe within the limited space of the sternotomy to realize the selected echocardiographic view. The success of an acquisition was therefore determined off-line based on SW visibility and signal strength, and IVS orientation in the ARF-based SW measurements. Time traces of the active SWS estimations were temporally matched by manually selecting the onset of the diastolic phase. Subsequently, the SWS traces of successful active SWE acquisitions and corresponding passive SWE acquisitions were separately averaged per animal, regardless of the chosen push and/or imaging settings.

## III. Results

### A. Success rate of SWE acquisitions

Measurements with a poor probe contact and thus a poor image quality, or with a very unconventional orientation of the IVS were excluded. Furthermore, acquisitions with visibly no ARF-induced SWs over the heart cycle were discarded as well. This resulted in a relatively low success rate among all analyzed acquisitions per animal: 5/25 (20%), 1/14 (7%), 2/18 (11%) and 5/16 (31%) for Pig 1 to 4 respectively.

### B. Passive SWE

Fig. 1A shows M-panels obtained for the SWs induced after one AVC and MVC event in Pig 1. The median SWS together with the inter-quartile range (IQR) for the passive SWE sequence are visualized in Fig. 2 for each pig. For the AVC, we obtained median (IQR) SWS values of 2.5 (2.2 –

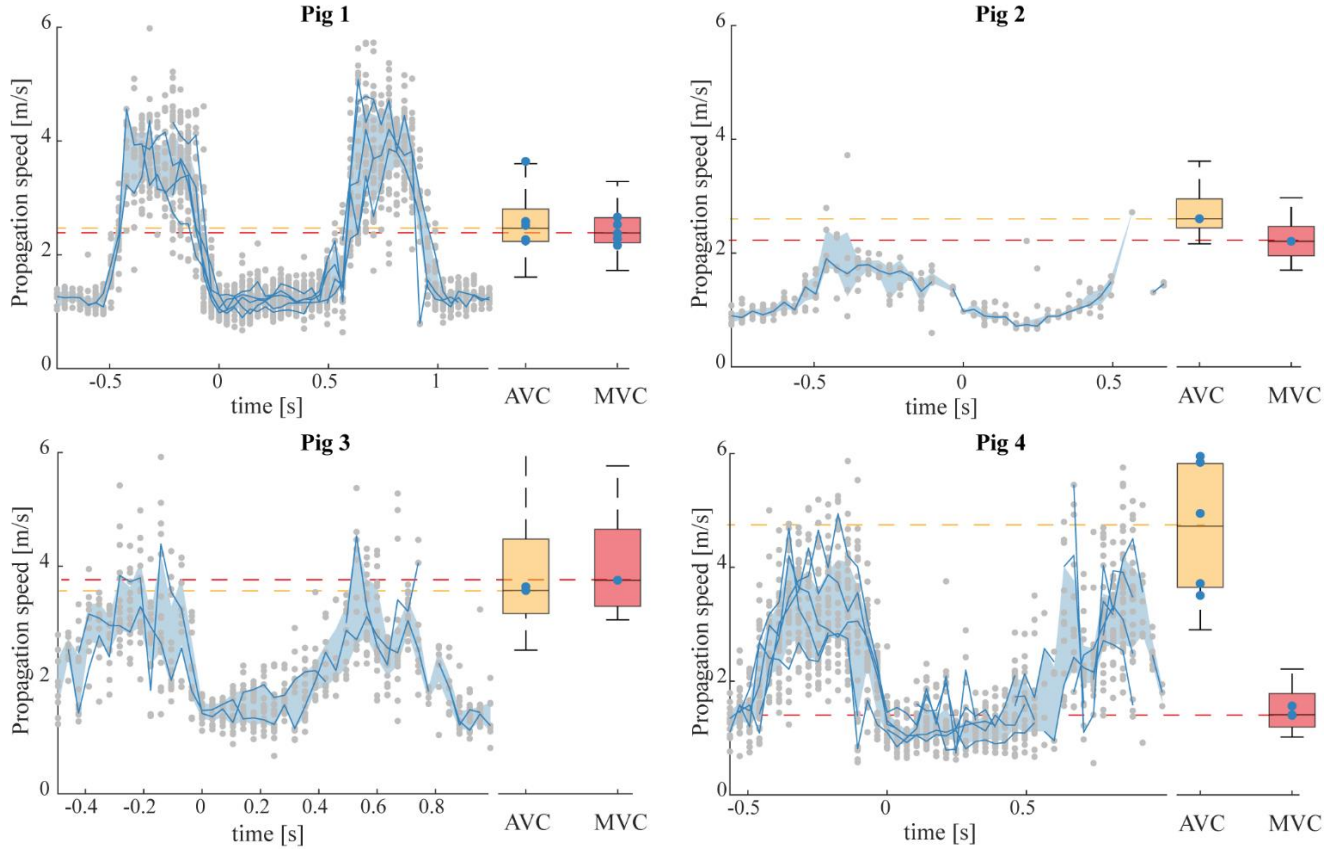


Fig. 2. Comparison of the propagation speeds obtained for consecutive ARF SWS and passive SWS measurements in 4 different animals (n=5, n=1, n=2 and n=5 for Pig 1 to 4 respectively). The curves over time correspond to the ARF SWS measurements. The boxplots correspond to the passive SWS measurements after AVC (orange) and MVC (red). The shaded areas depict the interquartile ranges of all values obtained for each individual animal. The blue curves and dots depict the median values for the different ARF SWS and passive SWS acquisitions respectively. The grey dots show the values obtained for the individual M-lines in the ARF SWS acquisitions (10 M-lines per acquisition).

2.8) m/s, 2.6 (2.4 – 2.9) m/s, 3.6 (3.2 – 4.5) m/s and 4.7 (3.6 – 5.8) m/s in Pig 1 – 4 respectively. For the MVC, these median SWS were found to be 2.4 (2.2 – 2.7) m/s, 2.2 (1.9 – 2.5) m/s, 3.7 (3.3 – 4.6) m/s and 1.4 (1.2 – 1.8) m/s.

### C. *Active SWE*

Fig.1B shows multiple M-panels obtained during an individual heart cycle of Pig 1. The M-panels show two SWs, one propagating from the push focus to the apex (upper SW) and one propagating from the push focus to the base (lower SW). Wave propagation speeds were determined for the SWs propagating to the apex.

Fig. 2 depicts the median SWS measured in each sequence over the cardiac cycle in the four animals. The blue shaded area depicts the IQR of all values obtained for all sequences. The higher range of measured SWS values varied between 3.2 – 4.5 m/s, 1.2 – 2.4 m/s, 2.5 – 4.2 m/s and 2.7 – 4.1 m/s (max. IQR) for Pig 1 to 4 respectively (presumably systole). For the lower range of SWS estimations, we obtained SWS variations (max. IQR) of 1.2 – 1.7 m/s, 1.1 – 1.3 m/s, 1.1 – 2.0 m/s and 1.0 – 1.6 m/s for Pig 1 to 4 respectively (presumably diastole).

### D. *Active vs Passive SWE*

For Pig 1, the SWS obtained for the AVC and MVC were in between the systolic and diastolic SWS of active SWE. For Pig 2, the SWS values after AVC and MVC were higher than the SWS values obtained with active SWE (+128%). Nonetheless, the passive SWS values are in the same range as found for Pig 1 and it should be noted that it was only feasible to obtain SWS values in one active SWE dataset. For Pig 3, both passive SWS values corresponded with the range of systolic SWS found with active SWE. For Pig 4, the SWS after AVC were in the range of the systolic SWS of active SWE, whereas the SWS after MVC corresponded better with the diastolic SWS of active SWE.

By chance, the passive SWs induced by the AVC and/or MVC were also visible in some M-panels of the active SW measurements, such that we had a near-simultaneous active and passive SWE readout. The results of the SWS analysis of these passive SWs within the active measurements for the same M-lines as used for the active SWs, is shown for one representative acquisition in Fig. 3. The same post-processing settings were used as for the separate passive acquisitions. Fig. 3 shows a very good match between the active and passive SWS. Additionally, this figure demonstrates a clear difference

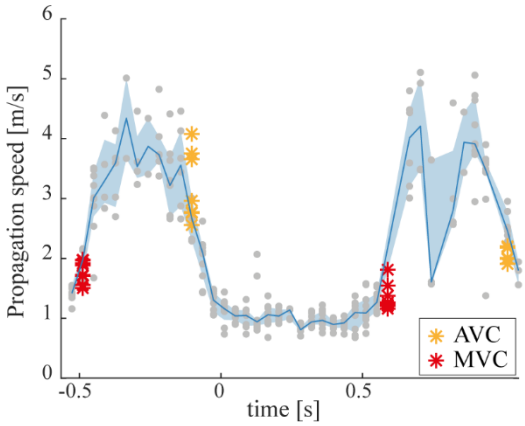


Fig. 3. Comparison of the SWS obtained for the active and passive SWs in a single sequence for Pig 4. The shaded area depicts the interquartile ranges of the values obtained for the 10 M-lines. The blue curve depicts the median value. The grey dots show the values obtained for individual M-lines.

in SWS values for AVC for two subsequent heart cycles (median SWS of 3.0 m/s vs. 2.0 m/s for AVC; 1.9 m/s vs. 1.3 m/s for MVC).

## IV. Discussion and Conclusion

This study compared propagation speeds of shear waves (SWs) induced by acoustic radiation force throughout the cardiac cycle and natural SWs induced by aortic and mitral valve closure (AVC, MVC). Even though natural SWs have a longer wavelength (~5 vs. ~1 cm) and are induced by a complex source in space and time compared to active SWs, natural shear wave speeds (SWS) were found to be in the same range as the SWS in active shear wave elastography (SWE) measurements, as shown in Fig. 2.

The natural SWs induced after MVC and AVC occur during the isovolumic contraction and relaxation phase respectively. During these phases, we measured large changes in active SWS estimations, as visible in Fig. 2. Since active and passive SWE were consecutively performed, both sequences were acquired in different heartbeats and could therefore not be directly matched in time. For example, for Pig 1, the magnitude of the passive SWS was in between the systolic and diastolic SWS obtained by active SWE, whereas for Pig 4, the SWS after MVC and AVC were in the same range as the active SWS in systole and diastole respectively (see Fig. 2). Differences in post-processing settings (e.g. selected M-line) and analyzed heartbeat could potentially explain the differences between passive and active SWS among the four animals. Indeed, when tracking the passive SWs in the active SW acquisition for the same M-lines, we obtained an excellent correspondence between active and passive SWS values, as displayed in Fig. 3. The results in Fig. 2 and 3 also suggest a large inter-heartbeat variability among the measured passive SWS values.

Even though currently applied sequences and processing settings differed in each SWE acquisition, the obtained SWS in the current study is in the same range as previously reported for active SWE in open-chest sheep (1.45 – 4.8 m/s [4]) and passive SWE in closed-chest pigs (2.2 m/s for MVC and 4.2 m/s for AVC [8]). Future work should investigate optimal sequence and processing settings for active and passive SWE individually. Due to the low SNR in active SWE, SWS were manually determined to obtain a more robust SWS estimate, but this method is time-consuming and not very accurate. Additionally, the SWS results were less reliable in the systolic phase (as is clear from the larger obtained IQR in systole than in diastole in Fig. 2 and 3), where the number of frames displaying shear wave propagation are limited due to the reverberation and the high SWS magnitude. Furthermore, as the nature of the presented study is invasive in anesthetized animals, it is unsure how representative obtained SWS values are for a closed-chest setting.

The open-chest feature of the current study allowed to measure the dynamic variation of cardiac stiffness using active SWE. However, probe contact and orientation issues resulted in a low success rate for active SWE, as reported in section III.A. The feasibility of passive SW tracking after valve closure is in general higher due to the larger tissue velocity magnitude (~40 vs. ~5 mm/s). Furthermore, the implementation of passive SWE in current clinical echocardiographic systems is expected to be easier than active SWE. Nonetheless, the interpretation of the passive SWS values is more difficult, as the results of current study demonstrated that the measured SWS value will be in between diastolic and systolic SWS and the timing of valve closure with respect to cardiac stiffness variation might be varying between heartbeats. Whether these passive SW measurements can be used to measure changes in relaxation/contraction and loading conditions should be further investigated.

## Acknowledgment

We thank the Experimental Cardiology group at the Erasmus MC, Rotterdam, the Netherlands for facilitating the animal experiments.

## References

[1] A. Petrescu et al., “Velocities of Naturally Occurring Myocardial Shear Waves Increase With Age and in Cardiac Amyloidosis,” JACC Cardiovasc. Imaging, vol. in press, 2019.

[2] M. Strachinaru et al., “Naturally Occurring Shear Waves in Healthy Volunteers and Hypertrophic Cardiomyopathy Patients,” Ultrasound Med. Biol., vol. 45, no. 8, pp. 1977–1986, 2019.

[3] O. Villemain et al., “Myocardial Stiffness Evaluation Using Noninvasive Shear Wave Imaging in Healthy and Hypertrophic Cardiomyopathic Adults,” JACC Cardiovasc. Imaging, vol. 12, no. 7, pp. 1135–1145, 2019.

[4] M. Couade et al., “In Vivo Quantitative Mapping of Myocardial Stiffening and Transmural Anisotropy During the Cardiac Cycle,” IEEE Trans. Med. Imaging, vol. 30, no. 2, pp. 295–305, 2011.

[5] P. Song et al., “Improved Shear Wave Motion Detection Using Pulse-Inversion Harmonic Imaging With a Phased Array Transducer,” IEEE Trans. Med. Imaging, vol. 32, no. 12, pp. 2299–2310, 2013.

[6] P. Hollender, V. Kakkad, and G. Trahey, “Calibration of ARFI displacements using diastolic shear wave speeds for estimating systolic elasticity,” in IEEE International Ultrasonics Symposium, Washington DC, 2017.

[7] B. Brekke et al., “Ultra-High Frame Rate Tissue Doppler Imaging,” Ultrasound Med. Biol., vol. 40, no. 1, pp. 222–231, 2014.

[8] H. J. Vos et al., “Cardiac Shear Wave Velocity Detection in the Porcine Heart,” Ultrasound Med. Biol., vol. 43, no. 4, pp. 753–764, 2017